JOURNAL OF COMPUTATIONAL PHYSICS 118, 152–158 (1995)

Finite-Grid Instability in Quasineutral Hybrid Simulations*

P. W. RAMBO

University of California, Lawrence Livermore National Laboratory, P.O. Box 808, Livermore, California 94550

Received January 24, 1994; revised October 12, 1994

Analysis and simulation of numerical instability caused by the spatial grid is presented for the case of quasineutral hybrid plasma simulation. The simplest case of particle ions advanced in the ambipolar electric field due to an isothermal, charge neutralizing electron fluid is examined. Stationary plasma is destabilized by finite ion temperature with the threshold temperature T_i characterized by the ratio ZT_e/T_i, where Z is the charge state of the ions and T_e is the electron temperature. A cold drifting plasma is found to be unstable with typical growth rate $\gamma \approx 0.4$–$0.6\ C_s/\Delta x$ (Δx is the grid spacing and C_s is the ion acoustic speed); simulations show that unstable growth is saturated by particle trapping leading to heated ions. For nearest grid point weighting, saturation, and threshold for growth are observed to be $T_i \approx 0.6\ ZT_e$ while for linear particle weighting, $T_i \approx 0.1\ ZT_e$. These results are relevant to hybrid particle simulations of laser generated plasmas, a regime where $ZT_e/T_i \gg 1$ is encountered.

I. INTRODUCTION

Hybrid simulations, which model some physical species with particles and others with fluids, have been applied to a wide variety of problems in magnetically confined fusion plasmas and space plasma physics. Typically the regime of interest is such that the ions are essentially collisionless and require a kinetic treatment while the electrons may be represented by a fluid. Although not necessary, these models are often designed to elliminate the fastest physical time scales to enable efficient simulation of longer time phenomena. Thus quasineutrality is often assumed, allowing a reduced treatment of the electrons. Further approximations, such as the Darwin approximation to electromagnetics, remove restrictions due to the Courant limit on light waves. The literature reports a wide variety of specific implementations [1] with emphasis on time stability which is an important concern for these algorithms.

No work, however, has been reported concerning effects of the finite spatial grid on such simulations. This is in sharp contrast to algorithms which explicitly resolve electrostatic plasma waves and electromagnetic waves, where analysis and simulation results for finite grid effects are well known [2]. In particular, the nonphysical electrostatic instability of a plasma interacting with the computational grid [3] has been extensively studied and can be an important limitation of these methods. Instability is caused by interaction between the physical wave at the plasma frequency ω_{pe}, and aliases displaced integral multiples of the grid wavenumber $k_g = 2\pi/\Delta x$, where Δx is the grid spacing. For the usual momentum conserving implementation, this instability leads to heating of cold plasmas, until stabilized by finite temperature characterized by the ratio of $v_{te}/(\omega_{pe}\Delta x)$, v_{te} the electron thermal velocity. The temperature at saturation is also the threshold for instability, with no unstable growth observed when the simulation is started with temperature above this value. This critical temperature is a function of the plasma drift velocity u_0, and for linear particle weighting is given by $v_{te} \approx 0.25\ \omega_{pe}\Delta x$ for non-drifting thermal (Maxwellian) plasma and $v_{te} \approx 0.046\ \omega_{pe}\Delta x$ for fast drift, $u_0 \gtrsim 0.3\ \omega_{pe}\Delta x$.

In this work, the linear stability and nonlinear heating and saturation of quasineutral hybrid simulations is investigated with respect to the finite computational grid. A simplified system is considered, one-dimensional in x, consisting of particle ions with charge Ze and mass M, and quasineutral isothermal electrons at temperature T_e. In the absence of collisions and magnetic field, the ions are advanced simply by

$$\frac{dx}{dt} = v, \quad \frac{dv}{dt} = \frac{ZeE}{M}$$

with the ambipolar electric field, E, derived from the electron fluid momentum equation neglecting inertia. In the absence of magnetic fields and assuming no current, this electric field is given by

$$E = \frac{-T_e}{en_e}\frac{\partial n_e}{\partial x} = \frac{-T_e}{en_i}\frac{\partial n_i}{\partial x}, \tag{1}$$

where the electron and ion charge densities are approximately equal due to the assumption of quasineutrality, $n_e \approx Zn_i$. This simple field equation contains the necessary physics and is representative of more complete field algorithms when electromagnetics are not important.

* The U.S. Government's right to retain a nonexclusive royalty-free license in and to the copyright covering this paper, for governmental purposes, is acknowledged.

0021-9991/95 $6.00

These equations and their numerical implementation may be cast in dimensionless form by normalizing distance to the grid spacing Δx, velocities to the ion acoustic speed $C_s \equiv (ZT_e/M)^{1/2}$, and time to $\Delta x/C_s$. Thus it is reasonable to expect that the critical parameters will be the drift velocity u_0 and ion thermal velocity $v_{ti} = (T_i/M)^{1/2}$ relative to the ion acoustic speed. It will be shown that instability occurs when the ion thermal velocity relative to the acoustic speed is smaller than a critical value and that unstable waves grow until saturated by particle trapping which heats the ions to a temperature proportional to ZT_e. These results can be anticipated by replacing electron quantities in the usual finite grid results quoted above with corresponding ion quantities, noting that the electron plasma frequency should be replaced by the ion acoustic frequency $\omega_s = kC_s \sim \pi C_s/\Delta x$, thus cancelling dependence on the grid spacing.

The results of linear analysis accounting for finite grid effects are presented in Section II, including numerical solutions of the dispersion relation. Section III presents stimulation tests showing heating and nonlinear saturation; additionally, the effect of ion–ion collisions is considered. Conclusions and remarks are to be found in Section IV, along with a realistic example relevant to laser produced plasmas.

II. LINEAR ANALYSIS

A simple one-dimensional periodic system is considered, with spatial grid given by $X_j = j\Delta x$, Δx the grid spacing. We will linearize about an equilibrium in which the plasma is assumed uniform with ion density n_0 and electrons and ions drift together with velocity u_0. The ions of charge Ze and mass M are represented by particles whose density is accumulated to the grid using standard particle in cell weighting, with shape function $S(x)$. The electric field on the grid, E_j, is interpolated back to the particles in a similar way to evaluate the acceleration. We will consider both nearest grid point (NGP) and linear (or cloud in cell, CIC) weighting. Since we are only concerned with effects of the spatial grid, we will ignore the time discretization and assume that relevant frequencies are adequately resolved.

Given the ion density on the grid, we must define the spatial differencing of Eq. (1) to determine the electric field on the grid. Two choices are apparent, the first being centered two-cell differencing,

$$E_j = \frac{-T_e}{en_j}\frac{(n_{j+1} - n_{j-1})}{2\Delta x} \tag{2a}$$

and the second being differencing of adjacent cells with an average to the cell center,

$$E_{j+1/2} = \frac{-T_e}{e}\frac{(n_{j+1} - n_j)}{\Delta x(n_{j+1} + n_j)/2}, \quad E_j \equiv \frac{1}{2}(E_{j+1/2} + E_{j-1/2}). \tag{2b}$$

It is easily shown that both these implementations exactly conserve ion momentum. Furthermore, either algorithm gives the same result for the perturbation field after linearization,

$$\delta E_j = \frac{-Te}{en_0}\frac{(\delta n_{j+1} - \delta n_{j-1})}{2\Delta x}.$$

With this expression for the perturbed electric field, the methods of Ref. [2] are easily applied to determine the linearized dispersion relation for Fourier amplitudes varying as $\exp(ikx - i\omega t)$, characterized by wavenumber k and complex frequency $\omega = \omega_r + i\gamma$. For the case where the equilibrium ion distribution is given by a Maxwellian at temperature T_i and drifting with velocity u_0, the dispersion relation is found to be

$$\varepsilon(\omega, k) = 1 - \left(\frac{ZT_e}{T_i}\right)\left\{\frac{\sin(k\Delta x)}{(k\Delta x)}\right\}\sum_{p=-\infty}^{+\infty} S^2(k_p)\frac{k}{2k_p}Z'\left(\frac{\omega - k_p u_0}{\sqrt{2}|k_p|v_{ti}}\right) = 0 \tag{3}$$

$$\frac{ZT_e}{T_i} = \left(\frac{C_s}{v_{ti}}\right)^2, \quad C_s = \sqrt{ZT_e/M}, \quad v_{ti} = \sqrt{T_i/M}.$$

The sum in Eq. (3) is over alias wavenumbers, $k_p = k - pk_g$, where the grid wavenumber is $k_g = 2\pi/\Delta x$, Z' is the derivative of the plasma dispersion function [4], and $S(k)$ is the Fourier transform of the weighting function. For the limiting case of a cold drifting plasma, Eq. (3) reduces to

$$\varepsilon(\omega, k) = 1 - (kC_s)^2\left\{\frac{\sin(k\Delta x)}{(k\Delta x)}\right\}\sum_{p=-\infty}^{+\infty}\frac{S^2(k_p)\,k_p/k}{(\omega - k_p u_0)^2} = 0. \tag{4}$$

Equations (3) and (4) are generally valid for any choice of weighting function, but in the numerical solutions to follow the two most widely used choices will be considered, namely *nearest grid point (NGP) and linear (or cloud-in-cell, CIC)* weighting,

$$S(k) = \left\{\frac{\sin(k\Delta x/2)}{(k\Delta x/2)}\right\}^r \quad \text{with } r = 1 \text{ (NGP) or } r = 2 \text{ (CIC).}$$

These dispersion relations have been left in physical quantities for clarity, but may easily be cast into dimensionless form, showing that $\omega/(kC_s)$ is a function of $k\Delta x$, parameterized by the drift velocity scaled to the sound speed u_0/C_s, and the reciprocal ion temperature parameter ZT_e/T_i. Thus, anticipating that a threshold for instability exists, we expect it to be given as a critical value of ZT_e/T_i. These expressions are similar to those given in Ref. [3] for the case of oscillations at the electron plasma frequency ω_{pe}, except that now the physical mode is an ion acoustic wave at frequency $\omega_s = kC_s$. Qualitatively, similar results are obtained with instability caused by interaction between the real plasma ($p = 0$) and the $p \neq 0$ aliases which

are a result of the spatial grid and appear as fictitious beams. For the cold plasma with no drift, $u_0 = 0$, the sum over aliases in Eq. (4) may be performed giving identical results for both NGP and CIC weighting,

$$\left(\frac{\omega}{kC_s}\right)^2 = \left\{\frac{\sin(k\Delta x)}{(k\Delta x)}\right\}^2,$$

showing that the stationary cold plasma is stable.

Finite drift or ion temperature is destabilizing, and strongly growing modes may be identified with resonance of the $p = \pm 1$ aliases. Figure 1 presents solutions to the warm plasma dispersion relation (Eq. (3), keeping $|p| \leq 5$), showing instability for the case of zero drift, $u_0 = 0$. Growth of these modes, which is primarily due to resonance with the $p = +1$ alias, is stabilized for $ZT_e/T_i \approx 25$ with CIC weighting and for $ZT_e/T_i \approx 12$ with NGP weighting. Note that for both NGP and CIC the maximum growth rate first increases as ZT_e/T_i increases

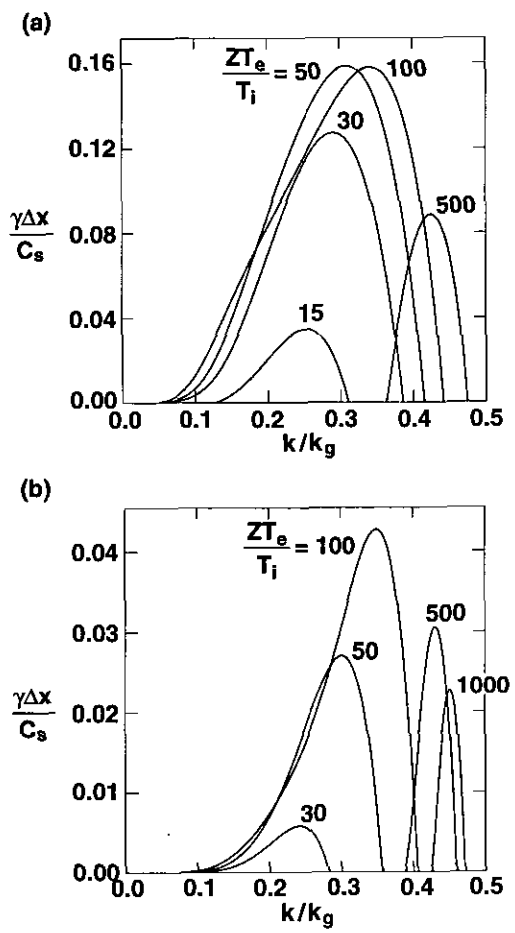

FIG. 1. Growth rates $\gamma\Delta x/C_s$ as a function of wavenumber k/k_g for stationary plasma, $u_0 = 0$ and various values of ZT_e/T_i: (a) NGP weighting and (b) CIC weighting.

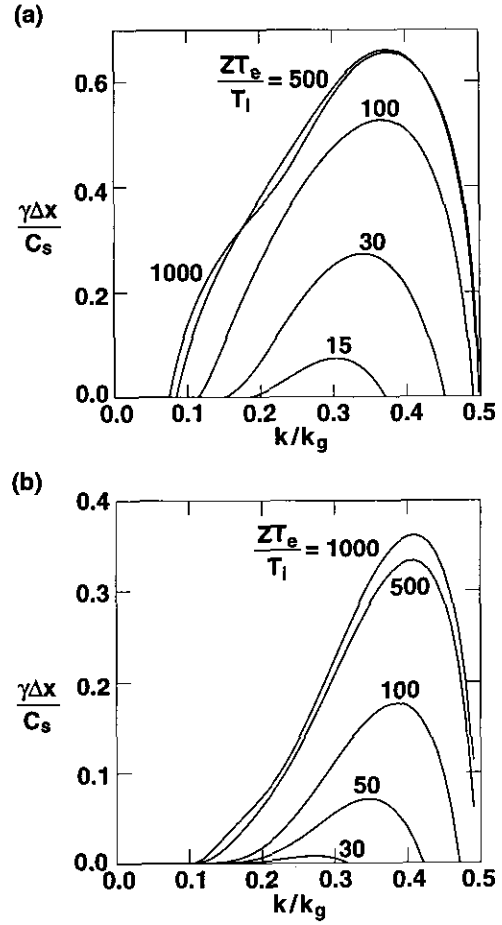

FIG. 2. Growth rates $\gamma\Delta x/C_s$ as a function of wavenumber k/k_g for drifting plasma, $u_0/C_s = 0.10$ and various values of ZT_e/T_i: (a) NGP weighting and (b) CIC weighting.

and reaches a maximum for $ZT_e/T_i \approx 100$. As ZT_e/T_i increases beyond 100, the maximum growth rate decreases and the unstable region moves toward larger values of k/k_g, approaching stability as ZT_e/T_i approaches infinity, corresponding to cold ions.

Finite drift substantially increases growth rates as shown in Fig. 2, where the drift velocity is $u_0/C_s = 0.10$. Again these modes correspond to resonance with the $p = +1$ alias, but modes resonant with the $p = -1$ alias have comparable growth rates. Note that the growth rate γ is a substantial fraction of $C_s/\Delta x$, which is the relevant time scale. As the drift velocity is further increased, the resonance with the $p = +1$ alias becomes dominant, and an approximate solution to the cold dispersion relation Eq. (4) can be found by keeping only the $p = 0$ and $p = +1$ terms. Assuming that the alias term is resonant, $\omega - k_p u_0 \equiv \delta\omega \approx 0$, one finds that

$$\left(\frac{\delta\omega}{kC_s}\right)^2 = \frac{S^2(k_p)(1 - k_g/k)\{\sin(k\Delta x)/(k\Delta x)\}}{\{1 - (kC_s/k_g u_0)^2 S^2(k)[\sin(k\Delta x)/(k\Delta x)]\}}$$

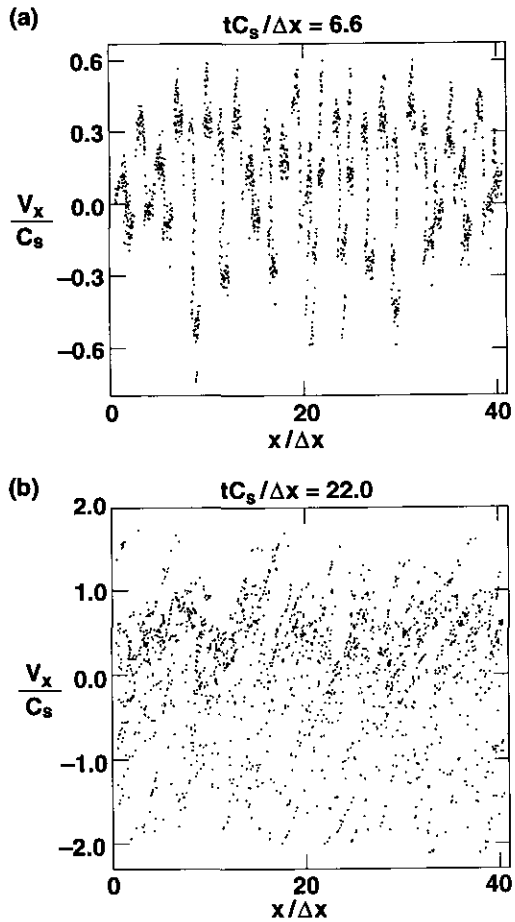

FIG. 3. Phase space v_x vs x from simulation using NGP weighting for $u_0/C_s = 0.10$, and initially $ZT_e/T_i = 600$ for times (a) $tC_s/\Delta x = 6.6$ during linear growth and (b) $tC_s/\Delta x = 22.0$ after saturation.

and $\delta\omega$ is purely imaginary when the denominator is positive. This is guaranteed for drift velocity exceeding the ion acoustic speed and for $u_0 \gg C_s$ the growth rate becomes independent of the drift velocity. In this limit, the growth rate becomes maximum at $k/k_g \approx 0.35$ with $\gamma\Delta x/C_s \approx 0.80$ for NGP weighting and $\gamma\Delta x/C_s \approx 0.38$ at $k/k_g \approx 0.41$ for linear weighting.

III. SIMULATION RESULTS

Simulations are now presented to illustrate growth and saturation of this unphysical instability. All the runs presented in this section are periodic of length 40 Δx and use 50 simulation particles per cell. The electric field is calculated using the spatial differencing of Eq. (2b); this choice was made for consistency with previous work on implicit multiple fluid plasma simulations [5]. The particles are advanced in time using the standard leap frog algorithm. As a first example, Figs. 3–4 show results from a drifting plasma with velocity $u_0/C_s = 0.10$ and using NGP weighting. The ions are given a small temperature to provide perturbations for the instability to grow from, initially $ZT_e/T_i = 600$. The time step is $C_s\Delta t/\Delta x = 2.2 \times 10^{-2}$ so that the relevant time scale is well resolved. Figure 3 presents snapshots of the particle phase space at two different times, showing the alias character of the instability during growth, as well as the later trapping at saturation. The time history of the thermal energy is presented in Fig. 4, clearly showing the gross violation of energy conservation. At saturation, the ion temperature in the simulation direction has heated considerably, $ZT_e/T_x \approx 1.6$; because the perpendicular velocities are constant, the temperature in the simulation direction is defined by

$$T_x \equiv M(\langle v_x^2 \rangle - u_0^2),$$

where the angular brackets denote an average over particles. Repeating this simulation with linear weighting also shows strongly growing instability, but saturation occurs at a lower level, $ZT_e/T_x \approx 13$, as shown by the dashed line in Fig. 4. Runs with stationary Maxwellians verify instability as predicted from linear theory; for NGP weighting starting from $ZT_e/T_x = 100$, heating to saturation with $ZT_e/T_x \approx 4$ is observed.

Figure 5 shows time histories of the ion temperature from several runs with NGP weighting, all with $ZT_e/T_i = 600$ initially, but with various values of u_0/C_s. For $u_0/C_s > 0.3$, the saturated ion temperature rapidly decreases, becoming approximately constant, $ZT_e/T_x \approx 25$ for $u_0/C_s > 1$ (a run with $u_0/C_s = 2$ is nearly identical to the run with $u_0/C_s = 1$ shown in the figure). This may be understood by considering the trapping limit of the unstable wave. As discussed in Ref. [3] the

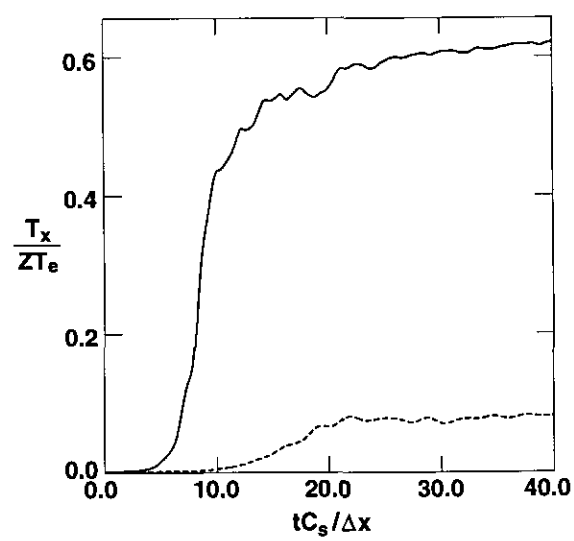

FIG. 4. Time history of thermal energy for simulation shown in Fig. 3 (solid line); dashed line shows result from equivalent simulation except using linear weighting.

thermal spread at trapping is estimated as $v_t \approx \gamma/k_p$, or $T_{sat} \approx M(\gamma/k_p)^2$. Substituting the values for maximum growth given at the end of Section II for the limit of $u_0/C_s \gg 1$, gives $T_{sat} \approx 0.04\ ZT_e$ for NGP weighting ($T_{sat} \approx 0.01\ ZT_e$ for CIC weighting), comparable to what is observed in Fig. 5.

As we have seen in both the linear theory of Section II and the simulations presented above, this instability has the greatest effect for large ZT_e/T_i which implies relatively cold ions with large charge state. This is precisely the regime for large ion–ion collision frequency (for sufficiently high ion density). To determine the effect of ion–ion collisions, several simulations have been performed with binary particle collisions. These collisions randomly pair up particles in a given grid cell and perform a momentum and energy conserving scatter for each particle pair [6]. For simplicity, these runs make use of completely isotropizing collisions; i.e., the angular scattering distribution in the center of mass frame is uniform in the solid angle. This might well be the situation encountered in more realistic simulations, where the Coulomb scattering rate is very large and not resolved by the simulation time step. Results from two such runs are shown in Fig. 6; parameters are $u_0/C_s = 0.10$ and initially $ZT_e/T_i = 600$. Because the particle collisions effectively isotropize the velocities within a cell, both parallel and perpendicular temperatures remain comparable. Although the saturated temperature is reduced compared to the collisionless case, instability and nonphysical heating are still present. This might seem somewhat surprising, since the collision frequency $\nu_c \approx 1/\Delta t = 45\ C_s/\Delta x$ is much larger than the growth rate. It should be born in mind, however, that these collisions only smooth velocity space and do not directly affect the density perturbations. Repeating the NGP simulation with the time step reduced a factor of 4 (collision rate increased a factor of 4) gives nearly identical results.

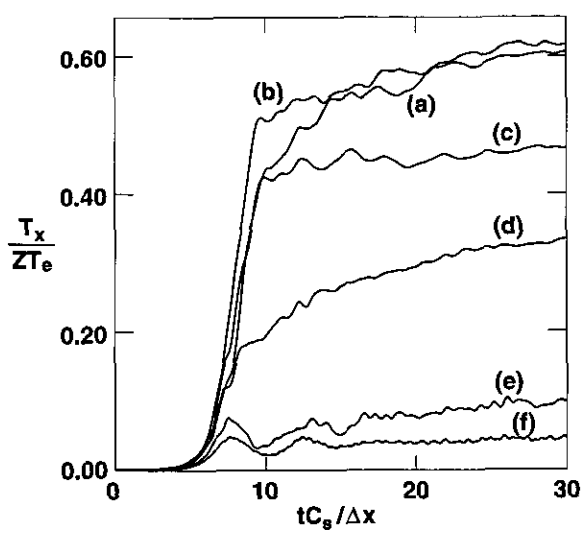

FIG. 5. Time histories of thermal energy for several simulations with different drift velocities: (a) $u_0/C_s = 0.10$, (b) $u_0/C_s = 0.20$, (c) $u_0/C_s = 0.30$, (d) $u_0/C_s = 0.40$, (e) $u_0/C_s = 0.60$, (f) $u_0/C_s = 1.0$. All simulations use NGP weighting and initially $ZT_e/T_i = 600$.

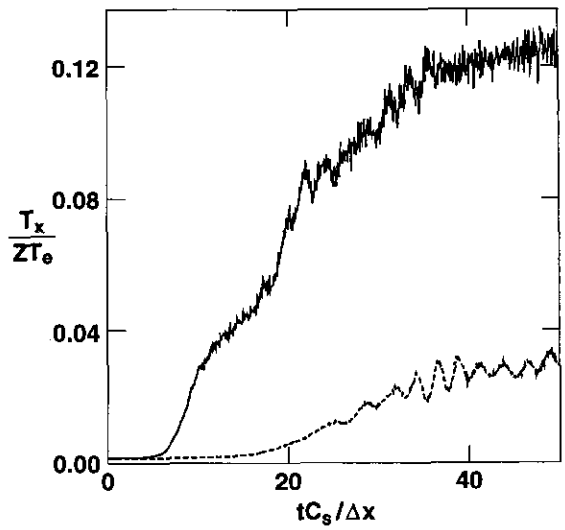

FIG. 6. Time history of thermal energy for simulations including isotropizing ion–ion collisions; $u_0/C_s = 0.10$ and initially $ZT_e/T_i = 600$. Solid line is from simulation using NGP weighting and dashed line is CIC weighting.

IV. SUMMARY AND DISCUSSION

Analysis and simulation of the nonphysical instability due to finite grid aliasing for quasineutral hybrid simulation has been presented. Dispersion relations were derived for cold and warm drifting plasmas. A cold ion distribution with no drift relative to the grid is stable; finite ion temperature or drift is destabilizing. For sufficiently large ion temperature stability is again achieved. These results are qualitatively similar to the well known case of electron plasma oscillations destabilized by the finite grid, but because the physical mode is an ion acoustic wave, the relevant scaling is the ion thermal velocity relative to the ion acoustic speed, $(v_{ti}/C_s)^2 = T_i/ZT_e$. Solutions to the warm and cold dispersion relations have been presented. For drifting plasma with $ZT_e/T_i \geq 100$, typical growth rates are substantial, $\gamma\Delta x/C_s \approx 0.4$–$0.6$. Increasing ion temperature leads to stabilization at approximately $ZT_e/T_i \approx 12$ for NGP weighting and $ZT_e/T_i \approx 25$ for linear weighting. Simple simulations verify the instability and show saturation due to particle trapping and heating. For the case of $u_0/C_s = 0.10$, saturated temperatures are approximately $ZT_e/T_i \approx 1.6$ for NGP weighting and $ZT_e/T_i \approx 13$ for linear weighting.

It is clear from the analysis and simulations, that this instability is only of concern for the regime of ZT_e/T_i greater than unity. In the past, these models have typically been applied to problems with $Z = 1$ (or a few) and $T_i \approx T_e$, so it is not surprising that finite grid effects have not been a noticeable problem. Recently, however, quasineutral hybrid simulations have been applied to laser generated plasmas, with $Z \gg 1$ and

$T_i < T_e$ to investigate interpenetrating plasmas [7, 8]. Due to the high densities of interest ($n_i \approx 10^{18} - 10^{22}$ cm^{-3}) these simulations also include collisional effects, both ion–ion and ion–electron. Parameters picked for a multiple-fluid simulation [9] of interpenetrating plasmas provide an extreme example of the parameter range of interest, $T_e = 2.5$ keV, $Z = 50$ (partially ionized gold) and initially $T_i = 100$ eV, so that $ZT_e/T_i = 500$, a parameter regime, where the finite grid instability investigated here might preclude particle simulation.

Deleterious effects from this instability have been observed while simulating exploding foils of fully ionized carbon. Figure 7 shows snapshots from such a simulation. The simulation is initialized as a self-similar Gaussian expansion, with the initial scale length $L_0 = 200$ μm, velocity $u_0 = \sqrt{3}\, C_s x/L_0$, integrated carbon density $N_i = 1.38 \times 10^{19}$ cm^{-2}, $T_e = 1.5$ keV, and $T_i = 500$ eV. The time step is $\Delta t = 1.0$ ps, the spatial grid size is $\Delta x = 10$ μm and approximately 9000 particles are present initially; particle weighting is nearest grid point. In this simulation the electrons are isothermal to approximate continuous laser heating. Monte Carlo ion–ion and ion–electron Coulomb collisions are included (with the approximation that the Coulomb logarithm is constant, $\lambda_{ii} = \lambda_{ei} = 7.5$). For this run, the ion–ion collision frequency is approximately $\nu_{ii} \approx 2 \times 10^{13}$ s^{-1} at the center of the foil, decreasing in time due to the increasing ion temperature and decreasing density. Although the time step does not resolve this large collision rate, for colliding plasma runs with a second adjacent foil the interaction between the two foils is resolved [7]. The spatial profile of ion temperature (obtained from particle moments) shown in Fig. 7 clearly shows unphysical heating near the center of the foil;

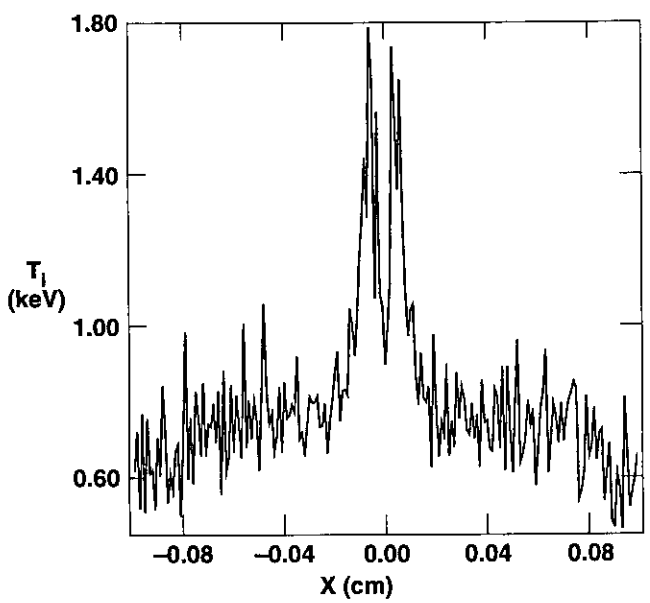

FIG. 7. Spatial profile of ion temperature at $t = 800$ ps taken from an exploding foil calculation using NGP weighting; initialization is described in text.

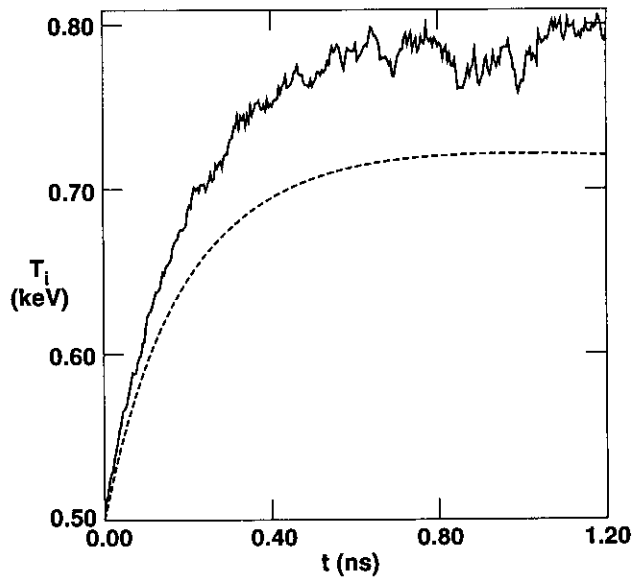

FIG. 8. Time history of ion temperature from center of exploding foil simulation using CIC weighting (solid line) compared to multiple-fluid simulation (dashed line).

evidence of the instability is just discernable in the particle phase space. For this case the instability appears to remain localized near the center of the foil, perhaps because of the increased velocity relative to the sound speed found away from the center. A simulation made with ion–ion collisions turned off shows much stronger signs of instability in phase space over the entire foil, although elevated ion temperature is still most pronounced near the center. Changing the particle weighting to linear has a beneficial effect, eliminating any obvious evidence of instability in both the spatial temperature profiles and phase space snapshots. Density oscillations are still observed, however, and the temporal history of the ion temperature (at the center of the foil) still shows higher values than for a fluid simulation as shown in Fig. 8. Increasing the number of particles a factor of 3 made no discernable difference, indicating that the source of the elevated ion temperature is not simply particle noise. Similarly, decreasing the time step a factor of four did not affect this result.

Thus we have shown that the finite grid instability investigated here can be operative in practical simulations. Using CIC weighting rather than NGP weighting improves the situation considerably. Although linear weighting is essentially standard in collisionless simulation, NGP has advantages for collisional fluid–particle interactions [10] and the optimum choice may best be left as problem dependent. Even with linear weighting, care must be exercised in applying quasineutral hybrid simulations to the regime $ZT_e/T_i \gg 1$. Higher order weighting can be expected to further improve stability, but with increased computational cost; spatial smoothing of the electric field might be a more attractive option. Still, particle simulation is a promis-

ing technique for physical situations which are transitioning between collisionless and collisional behavior, particularly for geometries where application of multiple-fluid techniques is difficult.

ACKNOWLEDGMENTS

The author acknowledges helpful discussions with J. Denavit, D. W. Hewett, A. B. Langdon, and R. J. Procassini. This work was performed under the auspices of the U.S. Department of Energy by Lawrence Livermore National Laboratory under Contract W-7405-Eng-48.

REFERENCES

1. D. W. Hewett and C. W. Nielson, *J. Comput. Phys.* **29,** 219 (1978); J. A. Byers *et al., J. Comput Phys.* **27,** 363 (1978); A. Mankofsky, R. N. Sudan, and J. Denavit, *J. Comput. Phys.* **70,** 89 (1987); D. W. Hewett, *J. Comput. Phys.* **38,** 378 (1980).
2. C. K. Birdsall and A. B. Langdon, *Plasma Physics via Computer Simulation* (McGraw–Hill, New York, 1985), p. 155.
3. C. K. Birdsall and N. Maron, *J. Comput. Phys.* **36,** 1 (1980).
4. B. D. Fried and S. D. Monte, *Plasma Dispersion Function* (Academic Press, New York, 1961).
5. P. W. Rambo and J. Denavit, *J. Comput. Phys.* **92,** 185 (1991); P. W. Rambo and J. Denavit, *J. Comput. Phys.* **98,** 317 (1992).
6. T. Takizuka and H. Abe, *J. Comput. Phys.* **25,** 205 (1977).
7. R. J. Procassini and P. W. Rambo, *Bull. Am. Phys. Soc.* **37,** 1520 (1992).
8. M. E. Jones *et al., Bull. Am. Phys. Soc.* **37,** 1521 (1992).
9. R. L. Berger *et al., Phys. Fluids B* **3,** 3 (1991).
10. Consistency between particle and fluid components is more easily achieved with NGP weighting; one aspect of this is briefly discussed in J. Denavit, "Time-Implicit Simulation of Particle-Fluid Systems," in *Space Plasma Simulation*, edited by M. Ashour-Abdalla and D. A. Dutton (Reidel, Boston, 1985), p. 85.